PAPER

An electrochemical sensor for flubendiamide insecticide analysis based on chitosan/reduced graphene oxide

S. Aghris,[a] M. Azriouil,[a] F. E. Ettadili,[a] A. Loukili,[b] F. Laghrib,[ac] A. Farahi,[a] M. Bakasse,[d] S. Lahrich[a] and M. A. EL Mhammedi [ID] *[a]

In the present work, a reduced graphene oxide/chitosan pencil electrode (rGO/CHI/PGE) was successfully synthesized for the analysis of flubendiamide (FBD). The graphene oxide (GO) was reduced by a quick, efficient, and green electrochemical method without the use of any reducing chemicals. Structural and morphological analyses of the rGO/CHI/PGE were carried out. Under optimized parameters, the detection limit was found to be 9 nM. This developed electrochemical device was successfully used as a simple and cost-effective electrode for FBD detection in white rice samples.

1. Introduction

Graphene, a single layer of carbon atoms arranged in a hexagonal honeycomb structure, has attracted many scientists because of its exceptional thermal, electronic, and mechanical characteristics. Graphene has been found to have excellent properties for different fields including electronic gadgets,[1] nanocomposites,[2] energy storage such as ultra-capacitors,[3–5] and batteries,[6] fuel cells,[7–11] solar cells,[12–14] and biotechnologies.[15–19] However, due to the high cost and difficulty of producing graphene, several efforts have been made to develop efficient and affordable processes to produce and use graphene derivatives, such as graphene oxide (GO). GO is highly stable in aqueous colloids because of the presence of oxygen functional groups, promoting the repulsive electrostatic interactions at the edges.[20] The two faces of the basal plane and the edges of GO can be laced with randomly dispersed oxygen groups,[21–27] while the basal plane is only occupied by epoxy and hydroxyl functional groups, and the edges are linked by carbonyl and carboxyl functional groups.[28–30] These oxygen-containing groups affect their electrochemical performance.[31,32] GO reduction is considered an interesting route to obtain a superconductor,

along with pure graphene. Various GO reduction methods, such as chemical, thermal and photothermal treatments, have been reported recently. However, most GO reduction methods require toxic reagents, huge energy consumption, and exceptional equipment. Different from the previously mentioned GO reduction methods, electrochemical technology is developed to offer a different alternative.[33] Electrochemical reduction of GO sheets pre-deposited on electrode surfaces offers a potential technique for preparing rGO-modified electrode surfaces.[33] The mechanisms of electrochemical exfoliation are primarily determined by the type of potential use. Anion species in the process of anodic exfoliation are intercalated into graphite. A positive current generates electrons from the graphite anode to form a positive charge at its surface,[34] and this charge activates the intercalation of bulky negative ions, like sulfate anions. These anions enhance the separation between graphene sheets and facilitate their exfoliation.[35] In cathodic exfoliation, a negative charge at a graphite working electrode draws ions to charge positively in the solution (*e.g.*, Li$^+$), and the intercalation opens the graphene sheets, resulting in expansion and exfoliation.[36] In this work, we promote an anodic exfoliation by applying a positive current in a Na_2So_4 electrolyte solution.

Chitosan (CHI), is a natural polysaccharide that contains two primary amino groups in the main polymer chain.[37] It has been largely used because of its exceptional characteristics, including non-toxicity, biocompatibility, hydrophilicity and antibacterial activity.[38] CHI is promoted as an effective adsorbent as it contains both amine and hydroxyl groups that can eliminate heavy metal ions by creating stable metal chelates.[39–41] The combination of graphene and chitosan can provide significant benefits in terms of high adhesion, good stability, excellent absorption capacity, and

[a] *Sultan Moulay Slimane University, Laboratory of Materials Science, Mathematics and Environment, Polydisciplinary Faculty, Khouribga, Morocco.*
E-mail: elmhammedi@yahoo.fr; Fax: +212 23485201; Tel: +212 68858296
[b] *Regional Center for Teaching and Training Professions, Laboratory of Scientific Research and Pedagogical Innovation, Rabat-Salé-Kénitra, Morocco*
[c] *Sidi Mohamed Ben Abdellah University, Laboratory of Engineering, Electrochemistry, Modeling and Environment, Faculty of Sciences, Fez, Morocco*
[d] *Chouaib Doukkali University, Organic Micropollutants Analysis Team, Faculty of Sciences, Morocco*

significant electrochemical detection performance.[42,43] In this context, Islam *et al.* synthesized CHI–graphene oxide films by dissolving CHI in 1% acetic acid and mixing an aqueous solution of CHI with GO suspension.[44] CHI and GO nanocomposites were formed from the addition of both components in aqueous media.[45] A simple solution-casting method was used to successfully prepare GO/CHI nanocomposites.[46] Wet spinning was used to create GO/CHI fibers, which were then used as adsorbents to remove fuchsin acid.[47] To achieve selective retention of divalent cations, a reduced GO and nanohybrid membrane was developed.[48] A new method for synthesizing composites by direct chemical exfoliation of graphite and CHI dissolved in acetic or aspartic acid was reported.[49]

The objective of this study is to provide an easy and inexpensive approach for the preparation of GO/CHIT composites to develop a sensitive electrochemical sensor for FBD detection. The prepared sensor exhibited a significant enhancement in electroanalytical performance for FBD reduction. Finally, the electrochemical sensor is used for the determination of FBD in real samples.

2. Experimental

2.1 Apparatus and reagents

For voltammetry experiments, a Metrohm/potentiostat coupled to 797 VA Computrace Software was used. The electrochemical apparatus consists of an rGO/CHI/PGE as the working electrode; pencils (HB Monami ML-SQ 0.7 × 60 mm) were purchased from a local bookstore, Ag/AgCl/KCl (saturated) was used as the reference electrode, and a platinum wire was used as a counter electrode. Flubendiamide 20% Wg (Tata TAKUMI) was purchased in an agricultural products store. The chitosan flake N 75% deacetylated molecular weight is about 310 000–375 000 Da (Merck (Darmstadt, Germany). The pH was measured using a sensION™ pH 31^m. Dibasic and monobasic potassium phosphates (purchased from sigma Aldrich) were used for the preparation of phosphate buffer solution, pH 7 (PBS 7). X-ray diffraction studies were performed using an XPERT-PRO diffractometer (XRD: Cu Kα radiation), (K_{Cu} = 1.54 nm). The diffraction angles (2θ) ranged from 10 to 80, with a step size of 0.008° per second. SEM observations were carried out using a JEOL JSM-IT500 HR scanning electron microscope.

2.2 Synthesis of graphene oxide

According to the experimental procedure reported by Loudiki *et al.*[50] and with slight modification in our optimized parameters, GO flakes were synthesized in aqueous electrolyte Na_2SO_4 (0.1 M). Briefly, two pencils were used as the anode and cathode to obtain GO flakes during the electrochemical exfoliation process. A static potential of +7 V was applied for 35 minutes, across both electrodes. Next, the sample was sonicated for 10 minutes, followed by centrifugation at 4000 rpm for 10 minutes to precipitate the

non-oxidized/exfoliated graphite, and the GO sheet suspensions were carefully extracted.

2.3 Preparation of GO/CHI

A chitosan solution was prepared by dissolving 200 mg of CHI in 50 mL of 1% acetic acid, and the mixture was stirred for 60 minutes at room temperature. The pH was adjusted to 5.0 with 1.0 M NaOH solution under vigorous agitation. Then, a specific amount of GO suspension was added to the CHI solution, and the mixture was sonicated for another 15 minutes.

2.4 Preparation of the rGO/CHI/PGE

With 500 fine grit sandpaper, the pencil lead was gently polished. Then, each pencil lead was immersed in 10 mL of composite contained in Eppendorf tubes for 30 minutes to form a layer of GO/CHIT on the surface of the PGE. The GO/CHIT modified PGE was then allowed to dry upside down for 15 minutes. Afterward, the electrochemical reduction was attained using CV by applying a potential range from −1.5 V to −0.2 V for 10 cycles in 0.1 M Na_2SO_4 at 50 mV (Scheme 1).

3. Results and discussion

3.1 Electrochemical anodic exfoliation

The experimental process of electrochemical anodic exfoliation of graphite is shown in Scheme 2. The process of exfoliation was carried out using two graphite leads as the anode and cathode in 0.1 M Na_2SO_4. By applying a DC voltage of 7 V, large bubbles formed at both electrodes with the dissociation of the anodic graphite (Scheme 2). Graphite layers were first intercalated by SO_4^{2-} and H_2O.[51] During the electrochemical process, self-oxidation of water and the reduction of SO_4^{2-} anions created SO_2 and O_2 gaseous species, which is shown by the rapid development of gases at the anode. Higher forces are generated between the layers of graphite by these gaseous species.[52] Finally, single-layer graphene sheets were formed by separating the weakly bonded graphite sheets from one another.

3.2 Electrochemical reduction of GO

Fig. 1 shows the cyclic voltammograms (CVs) of the GO/CHI deposit on the PGE in the range from −1.5 V to −0.2 V. One anodic peak appears at about −0.5 V during the process. In addition, this anodic peak decreases greatly and disappears in the 5th cycle. This confirms the deposition of the rGO/CHI composite on the PGE.[53–55] Therefore, the anodic peak is ascribed to some oxygen-containing groups on graphene planes.[56–59]
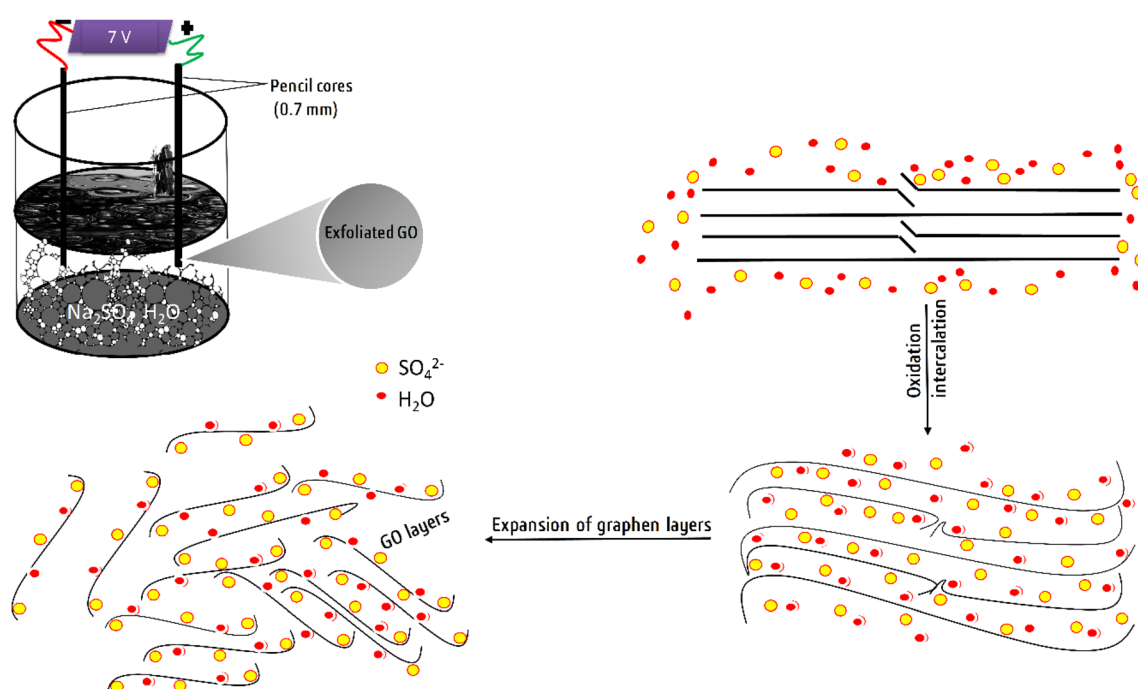
3.3 XRD and SEM analyses

XRD was carried out to study the crystallographic structure of CHI, exfoliated graphene oxide (GO), and the GO/CHIT composite in the 2θ range from 10° to 60° as shown in Fig. 2A. The CHI characteristic peak was observed at 2θ =
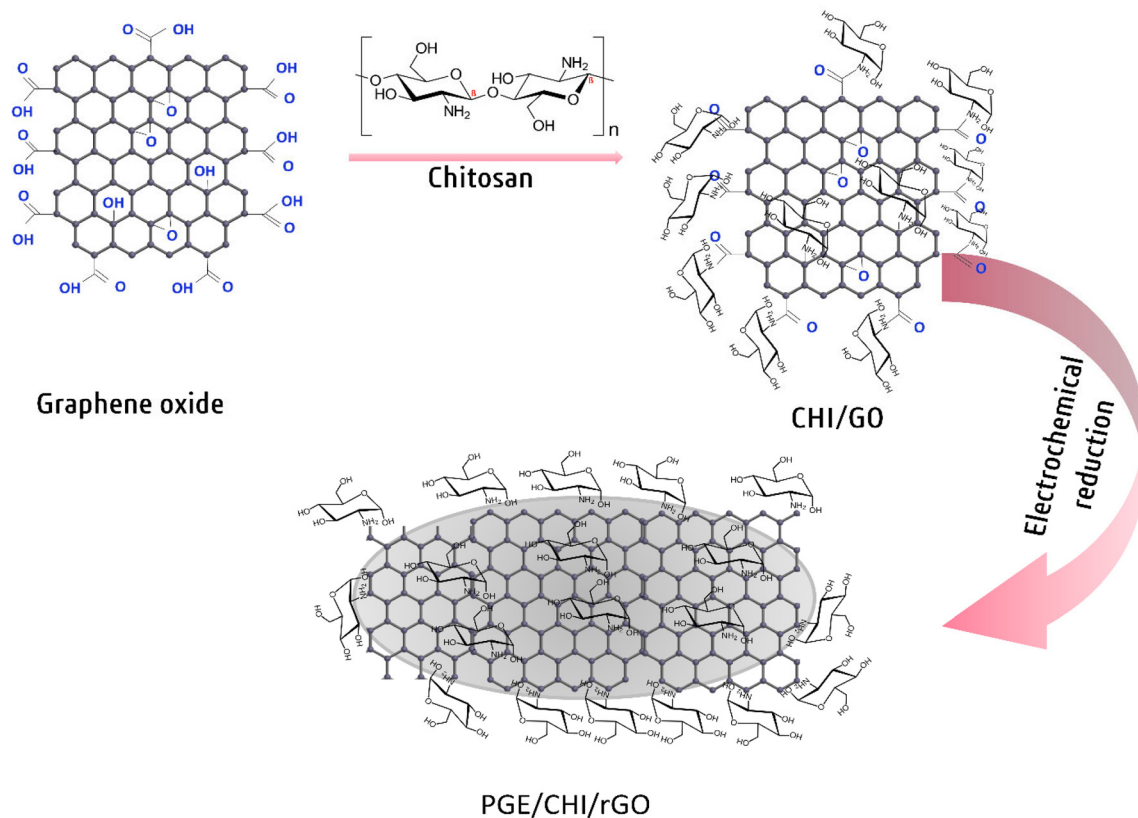
Scheme 1 Steps for rGO/CHI/PGE preparation.

Scheme 2 Experimental setup and the procedure for the electrochemical anodic exfoliation of graphite.

20.04° due to the semi-crystalline structures (110).[60] The initial exfoliated graphite displays a diffraction peak at $2\theta = 26.6°$. In the oxidation process, hydroxyl and epoxy groups separate carbon sheets primarily in the centers, while carboxyl groups are incorporated on the lateral sides of the sheets. The incorporation of these groups reduces the van
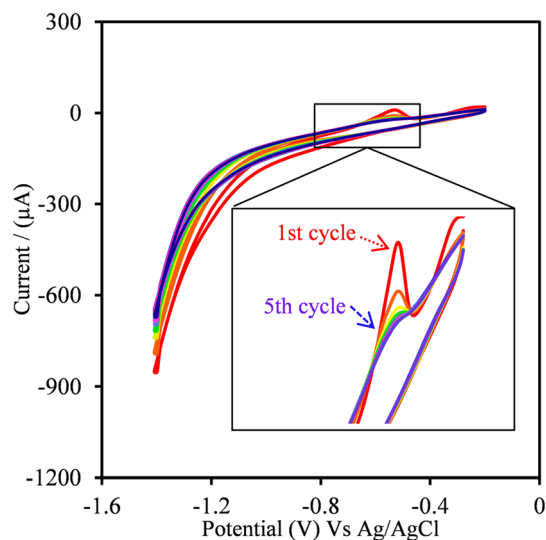
Fig. 1 CV voltammograms of the electrochemical reduction of graphene oxide in 0.1 M Na_2SO_4 at 50 mV s^{-1}.

der Waals forces between graphene sheets in the exfoliated graphene oxide.[61] The diffraction peak at $2\theta = 23.84°$ confirms the presence of rGO.[62] The broader peak at $2\theta = 19.8°$ corresponds to the (0 0 2) crystal plane of graphite and amorphous carbon.[63] There are also two very broad peaks around 32° and 33° attributed to the (004) reflection of graphene or graphite.[64] Furthermore, two weak peaks appeared at 48.48° and 54.52°, corresponding to the (100) and (004) reflection planes, respectively, related to the degree of crystallinity in amorphous graphene products.[65] It is observed that the position and the relative intensity of the diffraction peaks of GO change in the composite, which can be attributed to changes in the textural properties of the composites that are influenced by the presence of CHI in the corresponding material.

Fig. 2B–D show the SEM images of GO, CHI, and CHI/GO, respectively. The SEM image of exfoliated GO (Fig. 2B) shows a transparent layered structure, with few wrinkles on the surface. Fig. 2C reveals that the morphology of CHI features some holes and crevasses, in addition to the undefined internal structure. Fig. 2D reveals the coupling of the GO layers with CHI, and the presence of GO causes the
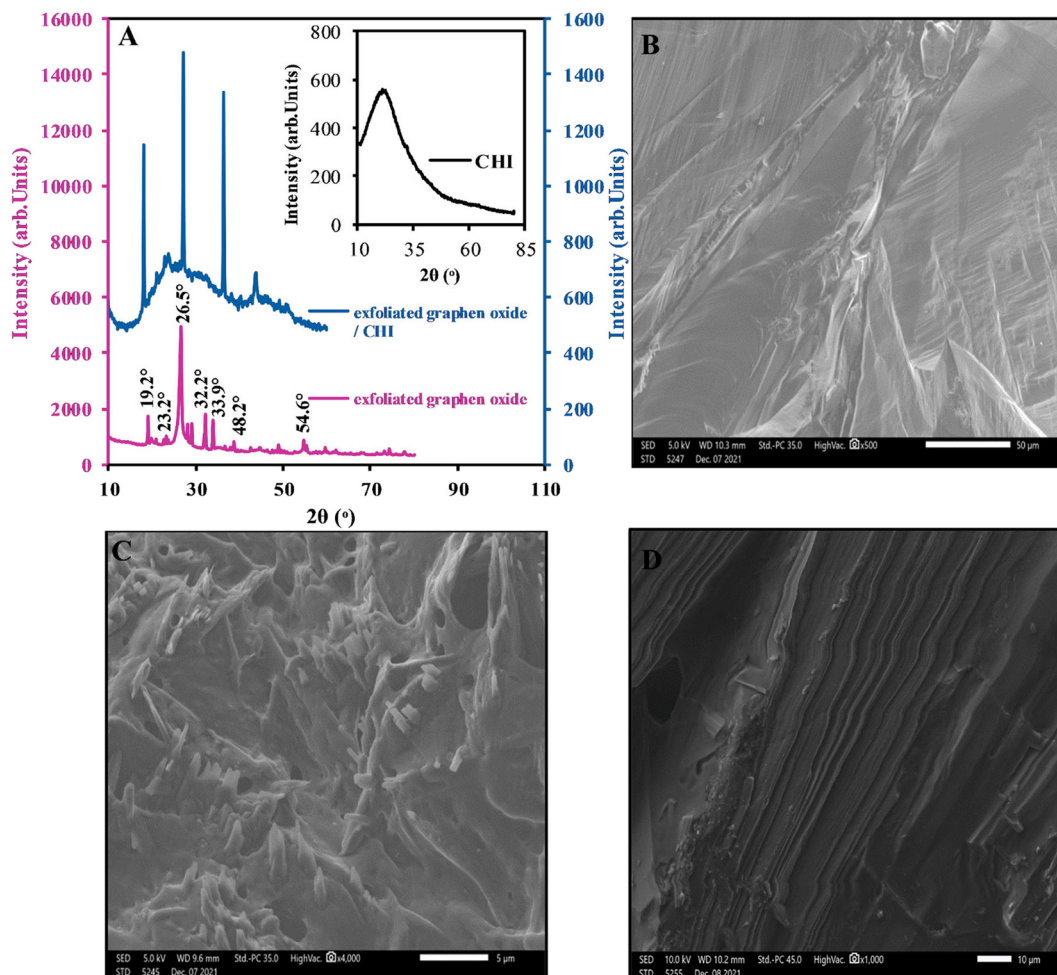

Fig. 2 (A) XRD analysis of exfoliated graphene oxide, CHI and GO/CHIT. SEM images of (B) GO, (C) chitosan, and (D) GO/CHIT.

formulation of well-organized tactoids of CHI/GO, which is manifested by the clear appearance of order stacking.

3.4 Electrochemical characterization

The electrochemical properties and the peak-to-peak separation values of the bare PGE, GO/CHI/PGE, and rGO/CHI/PGE were examined using the CVs in 0.1 M KCl containing 500 μM [Fe (CN)$_6$]$^{3/4}$. A redox peak appeared at the PGE bare as shown in Fig. 3A. The peak current improved after treatment of the PGE with GO/CHIT, indicating the improvement of electron transport on the electrode surface. However, compared to other modified electrodes, the redox peaks for the rGO/CHI/PGE exhibit the greatest peak currents.

Additionally, the scan rate effect of the rGO/CHI/PGE was examined by a CV technique at potential scan rates in the range of 10–500 mV s^{-1} Fig. 3B. The charge transfer coefficient (α) and heterogeneous electron transfer rate constant (k_s) in the reversible process were calculated by plotting the variation of the peak potential *versus* the logarithm of the scan rate (Fig. 3C).[66]

$$E_{pc} = E_0 - \frac{2.3RT}{\alpha nF} \frac{2.3RT}{\alpha nF} \log \frac{\alpha nF}{RT} \frac{\alpha nF}{RT} \times \frac{v}{K_s} \frac{v}{K_s} \quad (1)$$

According to eqn (1), the slope $S = -\frac{2.3RT}{\alpha nF} \frac{2.3RT}{\alpha nF}$ and Intercept $= E_0 + S \log \frac{-2.3}{S} \frac{-2.3}{S} - S \log(K_s)$.

α was calculated from the slope and found to be 0.62. The value of K_s was found to be 3.69 s^{-1}, by introducing values of α and E_0 in the intercept formula. The electroactive surface area of the bare PGE and modified electrodes was calculated using the Randles-Sevcik equation[67] (eqn (2)):

$$I_p = 2.69 \times 10^5 n^{3/2} AD_0^{1/2} C_0 v^{1/2} \quad (2)$$

By plotting I_{pa} *vs.* $v^{1/2}$ (inset Fig. 3B) and substituting these values in the above equation, the electroactive surface area was found to be 1.1×10^{-4} cm^2, 2.3×10^{-3} cm^2, and 8.35×10^{-3} cm^2 for the PGE, GO/CHI/PGE, and rGO/CHI/PGE, respectively. These findings demonstrate the fast electron transfer rates at the designed sensor surface.

EIS measurements were performed to assess the electron transfer properties of the electrodes. Fig. 3D shows the
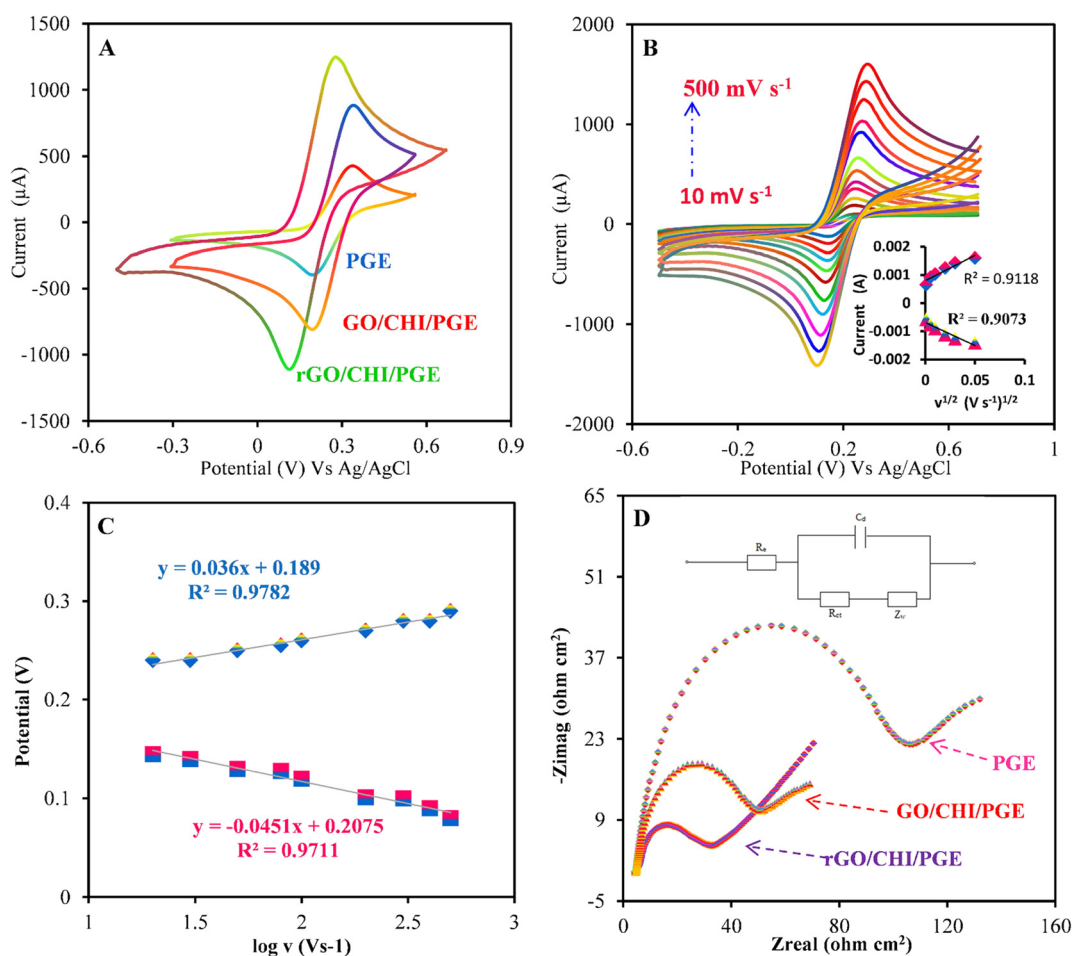

Fig. 3 (A) CV voltammograms of the PGE, GO/CHI/PGE, and rGO/CHI/PGE in 500 μM [Fe (CN)$_6$]$^{3-/4-}$ containing 0.1 mol L^{-1} KCl. (B) Cyclic voltammograms of rGO/CHI/PGE, and (inset) I versus $v^{1/2}$. (C) E versus log v at different scan rates from 10 to 500 mV s^{-1}. (D) EIS Nyquist plots obtained for the PGE, GO/CHI/PGE and rGO/CHI/PGE.

Nyquist plot of the rGO/CHI/PGE and the other electrodes. The inset in Fig. 3D illustrates the equivalent circuit, where R_s represents the resistance of the solution, R_{ct} signifies the transfer of charge, C_{dl} is the double-layer capacitance, and Z_w is the Warburg constant. R_{ct} was reduced from 108 Ω cm^2 (PGE) to 86 Ω cm^2 (GO/CHI/PGE) and 49 Ω cm^2 (rGO/CHI/PGE). This decrease is attributed to the modified electrode's capacity to hasten the electron transfer at the electrode surface (rGO/CHI/PGE).

The exchange current density values (j_o) were calculated using $j_o = RT/nFAR_{ct}$. The j_o value of the rGO/CHI/PGE was found to be equal to 0.641 mA cm^{-2}, which is higher than the j_0 values of 0.285 mA cm^{-2} and 0.207 mA cm^{-2} for the GO/CHI/PGE and PGE, respectively. Additionally, the semicircle's diameter at higher frequencies is equal to the electron transfer resistance R_{ct}. A considerable decrease in R_{ct} for the rGO/CHI/PGE compared to the bare PGE confirms the high electron transfer capacity of the synthesized composite.[68] In essence, the rGO/CHI/PGE has a lower R_{ct} and a higher j_o value, indicating that it is suitable for electrochemical applications.

3.5 Electrochemistry of FBD

Fig. 4A exhibits the DPV responses of the PGE, GO/CHI/PGE, and rGO/CHI/PGE in PBS pH 7.0 containing 300 μM FBD. A well-defined peak appears for the PGE attributing to the reduction of FBD. Afterward, the PGE was inserted into a CHI gel solution forming a film around the PGE, which is subsequently used for the detection of FBD for direct comparison. It was found that the peak reduction of FBD disappeared; this is because of the non-conductivity of CHI. To overcome the conductivity problem of the CHI/PGE, the use of rGO was highly required. Also, the natural structure of GO facilitates the insertion of small molecules or polymers between its layers. To achieve good dispersion, the anionic surface groups of GO interact with the CHI matrix by hydrogen bonding and electrostatic interactions. The prepared composite was demonstrated to be a promising sensor for FBD detection. In Fig. 4A, the reduction peak current at the GO/CHI/PGE was slightly increased due to the presence of oxygen-containing functional groups in GO. Thus, GO must be reduced to achieve similar unique properties to pristine graphene. Therefore, after the electrochemical reduction of GO (section 2.5), the experiments using the rGO/CHI/PGE show that the current peak increases almost two times compared to the PGE and GO/CHI/PGE. This indicates that GO reduction improves the electrical conductivity of the electrode and facilitates electron transfer.

The effect of the scan rate was studied to explain the electrochemical mechanism of FBD using the rGO/CHI/PGE
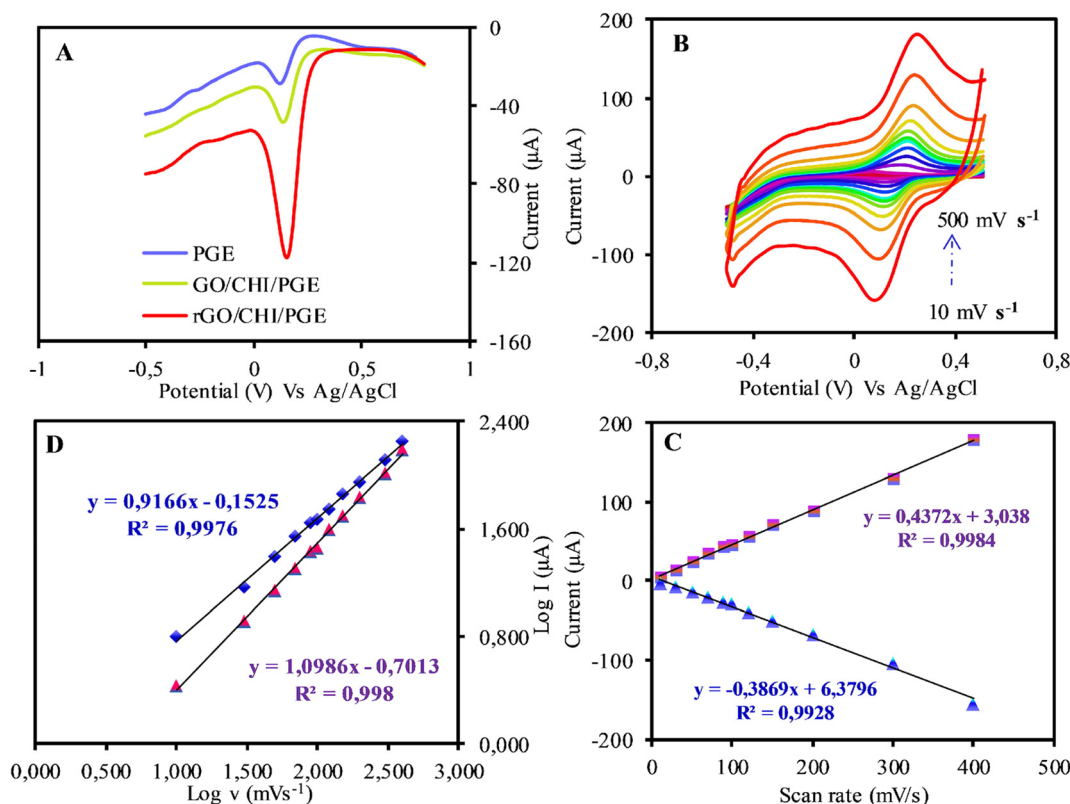

Fig. 4 (A) DPV voltammograms of the PGE, GO/CHI/PGE and rGO/CHI/PGE towards 300 μM FBD in 0.1 M PBS (pH 7.0). (B) Cyclic voltammograms of 300 μM FBD in PBS (pH 7.0) with the rGO/CHI/PGE at scan rates ranging from 10 to 500 mV s^{-1}. (C) I (μA) *versus* v (mV s^{-1}). (D) Log (I) against log (v).

electrode. The CVs were recorded in 300 μM FBD in PBS pH 7.0 at different scan rates in the range between 10 and 500 mV s^{-1} (Fig. 4B). The reduction peak current of FBD increases with the increase of the square root of the scan rate. Furthermore, when the scan rate increases, the peak potential of FBD slightly shifted toward a more negative potential. The cathodic peak current of FBD exhibit a linear relationship with scan rates ranging from 10 to 500 mV s^{-1} (Fig. 4C). According to these results, the electrochemical mechanism of FBD using the rGO/CHI/PGE electrode is a typical diffusion-controlled process. To support this argument, a linear correlation between the logarithm of the peak current (log I_{pa}) and the logarithm of the scan rates (log v) was obtained according to the following equations log I_{pc} = 0.9166 log v − 0.1525 (R^2 = 0.997) and log I_{pa} = 1.0986 log v − 0.7013 (R^2 = 0.998), for cathodic and anodic peak currents, respectively Fig. 4D. Corresponding to the above equations, the values of the slope are close to the theoretical value of 1, confirming that the reduction of FBD at the synthesized sensor is a diffusion-controlled process.

Afterward, the response of the rGO/CHI/PGE in 300 μM FBD at different pH was investigated in Fig. 5A. The obtained results for the cathodic and anodic peak current in pH ranging from 3.0 to 11.0 are shown in Fig. 5B and C. The results revealed that at pH 7.0, the cathodic and anodic responses of FBD were at their highest. These findings reveal that the rGO/CHI/PGE is suitable for a wider pH range, which is also convenient for FBD detection in real samples. Therefore, pH 7.0 was selected for subsequent measurements.

3.6 Effect of operational parameters

3.6.1. Effect of CHI percentage. The effect of the percentage of CHI on the detection of FBD was studied by

DPV recorded in 10 μmol L^{-1} of FBD. According to Fig. 6A, the amount of CHI appears to have an impact on the current response toward FBD, showing that the maximum peak current occurs at a percentage of 75%. These results show that despite the higher conductivity of GO, the presence of CHI remains very important in terms of the stability of GO layers.

3.6.2. Effect of incubation time. Various incubation times for the modified electrode were studied by DPV with 10 μmol L^{-1} of FBD, to assess the effect of incubation time on the electrochemical response. Fig. 6B illustrates that the peak currents increased with the increase in incubation time. From 60 to 500 s, there is a noticeable increase in current density; however, as the incubation time is prolonged, the increase in current density appears to be negligible. Therefore, regarding the duration of the experiments, the incubation time of 300 s was chosen.

3.7 Analytical determination of FBD at the surface of the rGO/CHI/PGE

Under the optimized parameters, the LOD determination of FBD on the rGO/CHI/PGE has been accomplished by the DPV technique (Fig. 7A). Fig. 7B shows a linear correlation of the FBD concentration in the range from 0.7 to 150 μM with a peak current (I_{pc}), R^2 = 0.9945. The sensor sensitivity was estimated by obtaining the slope of the calibration plot for the electrochemically active surface area, which was 0.00835 cm^2. The sensitivity of the rGO/CHI/PGE was found to be 47.3 μA μM^{-1} cm^{-2}. Following the IUPAC standards (3* σ/P) where σ is the standard deviation of the blank solution measurements and P is the slope, the sensor's limit of detection (LOD) was found to be equal to 0.009 μM. The efficiency of the rGO/CHI/PGE electrode was investigated by comparing its analytical performance with recently reported
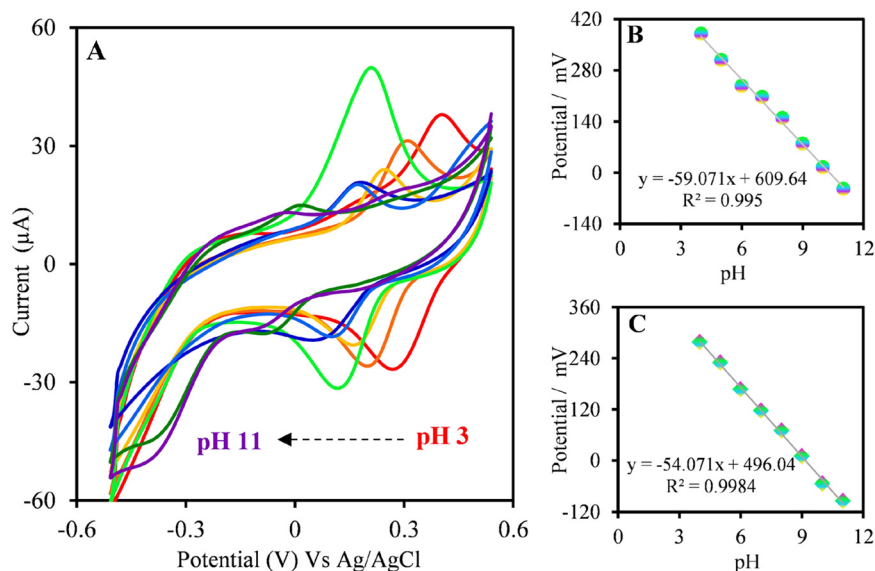

Fig. 5 (A) CVs voltammograms of the anodic and cathodic peaks at different pH values. (B) Plot of E_{pa} vs. pH value. (C) Plot of E_{pc} vs. pH value.
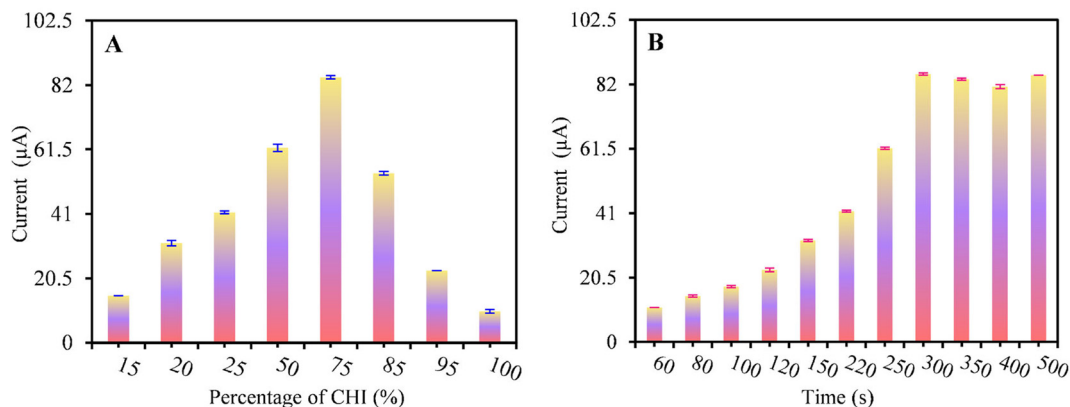
Fig. 6 (A) Optimization of the percentage of CHI and (B) optimization of incubation time.
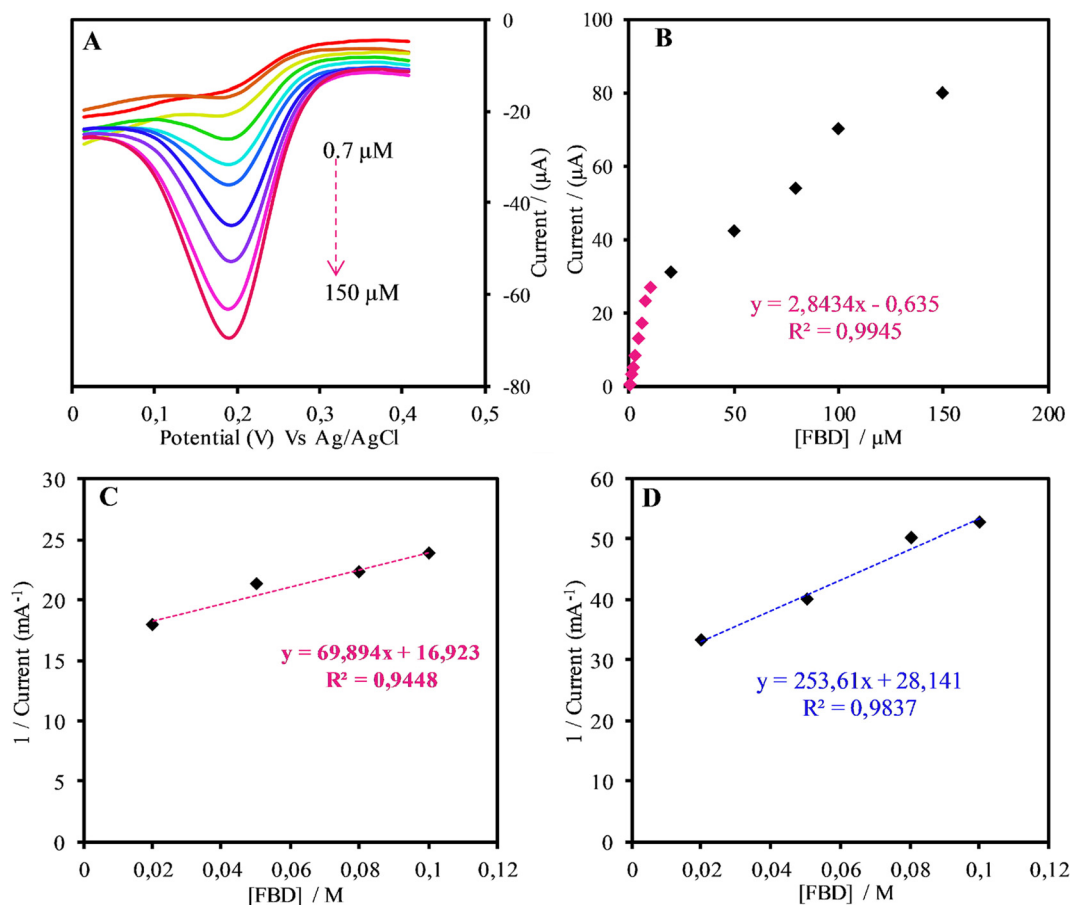

Fig. 7 (A) DPV voltammograms for increasing concentration of FBD from 0.7 to 150 μM under the optimized conditions using the rGO/CHI/PGE. (B) Linear relationship between I_{pc} and [FBD]. Linear calibration plots between peak current and concentrations of FBD with the (C) PGE and (D) rGO/CHI/PGE.

GO-based sensors for pesticide detection, as shown in Table 1. The listed findings reveal that the synthesized electrode has great analytical performance in terms of low LOD.[69–73] The manufactured rGO/CHI composite is regarded as a suitable and sophisticated electrode material for the sensitive and low-level detection of FBD. The reproducibility and the stability of the rGO/CHI/PGE were examined by using the DPV method in 10 μM of FBD. Seven modified PGEs were separately manufactured under the same conditions to investigate the reproducibility of the rGO/CHI/PGE. The results demonstrate that the synthesized electrode has good reproducibility, as indicated by the relative standard deviation (RSD = 2.54%). The rGO/CHI/PGE stability was also examined. On the same day, seven electrodes were

Table 1 Comparison of the recently reported graphene oxide sensors for the detection of pesticide

Electrode	Modifiers	Method	Linear range (μmol/L)	LOD (μmol/L)	Ref.
GCE	CS/GO-IIP	DPASV	0.5–100	0.15	69
AuE	Ag NPs/GO-CHIT/cyst	DPV	0.006–18	0.7	70
GCE	Chitosan/graphene	DPV	50–1200	50	71
GCE	Cu-CoNSs/CHIT-RGO	DPV	15–6950	10	72
GCE	PdNPs/GR/CS	DPV	100–4000	20	73
PGE	CHI/rGO	DPV	0.7–500	0.009	This work

GCE: glassy carbon electrode, CS/GO-IIP: chitosan/graphene oxide-ion-imprinted polymers, DPASV: differential pulse anodic stripping voltammetry, AuE: gold electrode, Ag NPs/GO-CHIT/cyst: silver nanoparticles/chitosan–graphene oxide/cysteamine, DPV: differential pulse voltammetry, Cu–CoNSs: copper–cobalt nanostructure, PdNPs/GR: a palladium nanoparticle/graphene.

manufactured. The electrochemical sensor's stability is satisfactory, as evidenced by the fact that after one week, 8% of the original response was reduced.

3.8 Binding affinity between the rGO/CHI/PGE and FBD

To analyze the binding affinity of FBD using the rGO/CHI/PGE and PGE, I_{max} *versus* FBD concentration was plotted in Fig. 7C and D. According to the DPV technique, the peak current is limited at a maximum value after achieving a concentration higher than 800 μM. The association constant (K) of FBD with CHI/rGO on the electrode surfaces can be calculated by using the following equation derived from the Langmuir isotherm (eqn (3)).[74]

$$\frac{[FBD]}{I_{pc}} = \frac{1}{KI_{max}} + \frac{[FBD]}{I_{max}} \tag{3}$$

where I_{pc} is the cathodic peak current for a given concentration of FBD, I_{max} corresponds to the maximum peak current, and K refers to the binding constant of FBD with CHI/rGO. $I_{pc(max)}$ reaches a consistent value of 56 μA and 35 μA using the rGO/CHI/PGE and PGE, respectively. The K values were calculated to be 2.86 and 0.78 M^{-1} for the rGO/

CHI/PGE and PGE respectively. These results confirm that CHI/rGO has the best recognition ability toward FBD molecules.

3.9 Selectivity

The selectivity of the rGO/CHI/PGE was analyzed in the presence of potentially interfering compounds such as pesticides and organic and inorganic molecules by using DPV. The sensor selectivity toward FBD was evaluated by adding 10 μM of FBD in the presence of imidacloprid, thiamethoxam, mancozeb, magnesium, sodium, and ascorbic acid. Table 2 shows that the investigated substances displayed an acceptable relative error on the modified electrode for the detection of FBD.

3.10 Application of the method in real samples

FBD was detected by using the electrochemical technique in white rice samples. An amount of 8 g was extracted with 10 mL of acetonitrile by using a vortex, followed by the rotational evaporation of 10 mL of the supernatant, and then diluted with PBS (pH 7). The extracted sample was transferred to the electrochemical cell, after filtration with a Buchner funnel. The linearity range, linear equations, correlation coefficients (R^2), LODs, LOQs, and RSD of white rice are listed in Table 3. The R^2 values demonstrate excellent linearity for the studied concentration range. The LOD and LOQ values were 0.24 μM and 0.84 μM, respectively, indicating the good sensitivity of the proposed method.

Table 2 Recovery of the interfering compounds for FBD determination using the rGO/CHI/PGE

Interfering	Concentration (M)	Recovery (%)
Magnesium	1.0×10^{-3}	100
	1.0×10^{-4}	100
	1.0×10^{-5}	100
Sodium	1.0×10^{-3}	99
	1.0×10^{-4}	100
	1.0×10^{-5}	99
Mancozeb	1.0×10^{-3}	100
	1.0×10^{-4}	99.8
	1.0×10^{-5}	101.5
Imidacloprid	1.0×10^{-3}	100
	1.0×10^{-4}	99
	1.0×10^{-5}	100.5
Thiamethoxam	1.0×10^{-3}	99
	1.0×10^{-4}	99
	1.0×10^{-5}	98
Ascorbic acid	1.0×10^{-3}	99
	1.0×10^{-4}	100
	1.0×10^{-5}	100

Table 3 Results for the determination of FBD in spiked white rice samples with the rGO/CHI/PGE using DPV

Parameters	rGO/CHI/PGE
Linear range (μM)	1–100
Intercept (μA)	5.3315
Slope (L mM)	30
Correlation coefficient (r^2)	0.9815
LOD (μM)	0.24
LOQ (μM)	0.84
RSD (%)	2.36

4. Conclusion

In the present study, an rGO/CHI/PGE sensor was designed for the detection of the FBD insecticide. The electrochemical investigation demonstrated the effectiveness of the rGO/CHI/PGE toward the electroanalytical reduction of FBD. The inclusion of rGO into CHI gel significantly increased the conductivity and improved electron the transfer characteristics. The fabricated electrochemical sensor showed high selectivity towards FBD. In particular, the results demonstrate that the manufactured electrode showed high electroanalytical activity, sensitivity, and stability in the FBD determination. The suggested approach provides a promising method for detecting FBD in samples of white rice.

Compliance with ethical standards

Ethical approval: S. Aghris, M. Azriouil, F. E. Ettadili, A. Loukili, F. Laghrib, A. Farahi, M. Bakasse, S. Lahrich, and M. A. EL Mhammedi declare that this study is ethically approved.

Informed consent: this article does not contain any studies with human participants or animals performed by any of the authors.

Data availability

The authors confirm that the data supporting the findings of this study are available within the article. Raw data that support the findings of this study are available from the corresponding author, upon reasonable request.

Conflicts of interest

S. Aghris, M. Azriouil, F. E. Ettadili, A. Loukili, F. Laghrib, A. Farahi, M. Bakasse, S. Lahrich, and M. A. EL Mhammedi declare that they have no conflict of interest.

References

1 J. Hass, W. A. De Heer and E. H. Conrad, *J. Phys.: Condens. Matter*, 2008, **32**, 323202.
2 D. Ponnamma, Y. Yin, N. Salim, J. Parameswaranpillai, S. Thomas and N. Hameed, *Composites, Part B*, 2021, **204**, 108493.
3 R. Kumar, S. Sahoo, E. Joanni and R. K. Singh, *J. Energy Chem.*, 2022, **74**, 252–282.
4 R. Lakra, R. Kumar, P. K. Sahoo, D. Thatoi and A. Soam, *Inorg. Chem. Commun.*, 2021, **133**, 108929.
5 M. Reina, A. Scalia, G. Auxilia, M. Fontana, F. Bella, S. Ferrero and A. Lamberti, *Adv. Sustainable Syst.*, 2022, **6**, 2100228.
6 S. Scaravonati, M. Sidoli, G. Magnani, A. Morenghi, M. Canova, J. H. Kim and D. Pontiroli, *Mater. Today Energy*, 2022, **24**, 100928.
7 H. Su and Y. H. Hu, *Energy Sci. Eng.*, 2021, **7**, 958–983.
8 Y. Han, H. Zhang, Z. Hu and S. Hou, *Energy*, 2021, **223**, 120095.
9 A. Alaswad, T. Wilberforce, A. Baroutaji and A. G. Olabi, *Encyclopedia of Smart Materials*, 2022, vol. 2, pp. 399–413.
10 J. Xia, Y. Geng, S. Huang, D. Chen, N. Li, Q. Xu and J. Lu, *J. Power Sources*, 2021, **512**, 230482.
11 C. Shi and X. Maimaitiyiming, *J. Alloys Compd.*, 2021, **867**, 158732.
12 S. Mahalingam, A. Manap, A. Omar, F. W. Low, N. F. Afandi, C. H. Chia and N. Abd Rahim, *Renewable Sustainable Energy Rev.*, 2021, **144**, 110999.
13 N. E. Safie, M. A. Azam, M. F. Aziz and M. Ismail, *Int. J. Energy Res.*, 2021, **45**, 1347–1374.
14 R. Ishikawa, S. Yamazaki, S. Watanabe and N. Tsuboi, *Carbon*, 2021, **172**, 597–601.
15 P. Thiyagarajan, *IET Nanobiotechnol.*, 2021, **4**, 348–357.
16 K. Pal, A. Si, G. S. El-Sayyad, M. A. Elkodous, R. Kumar, A. I. El-Batal and S. Thomas, *Crit. Rev. Solid State Mater. Sci.*, 2021, **5**, 385–449.
17 E. Mostafavi and S. Iravani, *Nano-Micro Lett.*, 2022, **1**, 1–12.
18 M. L. Verma, B. S. Dhanya, R. Saini, A. Das and R. S. Varma, *Environ. Chem. Lett.*, 2022, **20**, 1–24.
19 H. Kim, K. Solak, Y. Han, Y. W. Cho, K. M. Koo, C. D. Kim and T. H. Kim, *Nano Res.*, 2022, **15**, 9253–9263.
20 S. Mancillas-Salas, A. C. Reynosa-Martinez, J. Barroso-Flores and E. Lopez-Honorato, *Nanoscale Adv.*, 2022, **11**, 2435–2443.
21 H. M. Jung and S. Um, *Thin Solid Films*, 2016, **606**, 87–93.
22 B. Li, G. Pan, N. D. Avent, R. B. Lowry, T. E. Madgett and P. L. Waines, *Biosens. Bioelectron.*, 2015, **72**, 313–319.
23 K. Chaudhary, K. Kumar, P. Venkatesu and D. T. Masram, *Adv. Colloid Interface Sci.*, 2021, **289**, 102367.
24 B. Lesiak, G. Trykowski, J. Tóth, S. Biniak, L. Kövér, N. Rangam and A. Malolepszy, *J. Mater. Sci.*, 2021, **5**, 3738–3754.
25 A. Mathkar, D. Tozier, P. Cox, P. Ong, C. Galande, K. Balakrishnan and P. M. Ajayan, *J. Phys. Chem. Lett.*, 2012, **8**, 986–991.
26 T. Kuila, S. Bose, A. K. Mishra, P. Khanra, N. H. Kim and J. H. Lee, *Prog. Mater. Sci.*, 2012, **7**, 1061–1105.
27 C. N. Hernández, M. B. G. García, D. H. Santos, M. A. Heras, A. Colina and P. Fanjul-Bolado, *Electrochem. Commun.*, 2016, **64**, 65–68.
28 B. Gupta, N. Kumar, K. Panda, V. Kanan, S. Joshi and I. Visoly-Fisher, *Sci. Rep.*, 2017, **1**, 1–14.
29 Y. Long, J. Zhang, P. Li, J. Han, C. Geng and Q. H. Yang, *Encyclopedia of Energy Storage*, 2021, vol. 4, pp. 47–65.
30 J. M. L. del Río, E. R. López, F. García and J. Fernández, *J. Mol. Liq.*, 2021, **336**, 116885.
31 A. M. J. Haque, H. Park, D. Sung, S. Jon, S. Y. Choi and K. Kim, *Anal. Chem.*, 2012, **4**, 1871–1878.
32 M. Ding, H. Niu, N. Zhang, T. Hou, P. Guan and X. Hu, *Electrochim. Acta*, 2022, **425**, 140715.
33 Z. Aksu, C. H. Şahin and M. Alanyalıoğlu, *Sens. Actuators, B*, 2022, **354**, 131198.
34 M. Ikram, A. Raza, S. Ali and S. Ali, in *Sol Gel and other Fabrication Methods of Advanced Carbon Materials*, IntechOpen, 2020.

35 A. M. Abdelkader, A. J. Cooper, R. A. Dryfe and I. A. Kinloch, *Nanoscale*, 2015, **16**, 6944–6956.

36 S. Yang, M. R. Lohe, K. Müllen and X. Feng, *Adv. Mater.*, 2016, **29**, 6213–6221.

37 H. Jin and Z. Wang, *Macromol*, 2022, **3**, 346–360.

38 J. R. Neto, F. Copes, P. Chevallier, R. S. Vieira, J. V. L. da Silva, D. Mantovani and M. M. Beppu, *Colloids Surf., B*, 2022, **213**, 112359.

39 S. Rajabzadeh, G. H. Rounaghi, M. H. Arbab-Zavar and N. Ashraf, *Electrochim. Acta*, 2014, **135**, 543–549.

40 Y. Zuo, J. Xu, F. Jiang, X. Duan, L. Lu, H. Xing and Y. Yu, *J. Electroanal. Chem.*, 2017, **801**, 146–152.

41 B. Rezaei, H. R. Jamei and A. A. Ensafi, *Biosens. Bioelectron.*, 2018, **115**, 37–44.

42 H. Yuan, L. Y. Meng and S. J. Park, *Carbon Lett.*, 2016, **1**, 11–17.

43 Y. Areerob, C. Hamontree, P. Sricharoen, N. Limchoowong, S. Laksee, W. C. Oh and K. Pattarith, *RSC Adv.*, 2022, **24**, 15427–15434.

44 A. Islam, Y. H. Khan, A. Sarwar, N. Gull, S. M. Khan, M. A. Munawar and T. Jamil, *Carbohydr. Polym.*, 2016, **146**, 131–138.

45 M. S. Muda, A. Kamari, S. A. Bakar, S. N. M. Yusoff, I. Fatimah, E. Phillip and S. M. Din, *J. Mol. Liq.*, 2020, **318**, 114066.

46 A. Jadoon, Z. Ali, W. A. Farooq, F. Ali, G. J. Price, S. Taimur and S. Bibi, *Curr. Appl. Phys.*, 2022, **40**, 110–118.

47 C. Zhang, Y. Zhang, X. Hao, H. Liu, X. Lv, J. Zhu and Y. Zhang, *Adv. Compos. Hybrid Mater.*, 2018, **2**, 347–355.

48 Y. Wei, J. Wang, H. Li, M. Zhao, H. Zhang, Y. Guan and Y. Zhang, *RSC Adv.*, 2018, **25**, 13656–13663.

49 L. Magerusan, F. Pogacean, M. Coros, C. Socaci, S. Pruneanu, C. Leostean and I. O. Pana, *Electrochim. Acta*, 2018, **283**, 578–589.

50 A. Loudiki, M. Matrouf, M. Azriouil, A. Farahi, S. Lahrich, M. Bakasse and M. A. El Mhammedi, *Appl. Surf. Sci. Adv.*, 2022, **7**, 100195–100203.

51 Y. Orooji, H. Khojasteh, O. Amiri, M. Amiri, S. Hasanifard, S. Khanahmadzadeh and M. Salavati-Niasari, *J. Alloys Compd.*, 2020, **848**, 156495.

52 Y. Gong and C. Pan, *MRS Adv.*, 2017, **30**, 1611–1619.

53 S. Pei, Q. Wei, K. Huang, H. M. Cheng and W. Ren, *Nat. Commun.*, 2018, **1**, 1–9.

54 T. W. Chen, J. Y. Xu, Z. H. Sheng, K. Wang, F. B. Wang, T. M. Liang and X. H. Xia, *Electrochem. Commun.*, 2012, **16**, 30–33.

55 Z. Wang, X. Zhou, J. Zhang, F. Boey and H. Zhang, *J. Phys. Chem. C*, 2009, **32**, 14071–14075.

56 J. Ping, Y. Wang, K. Fan, J. Wu and Y. Ying, *Biosens. Bioelectron.*, 2011, **1**, 204–209.

57 L. Chen, Y. Tang, K. Wang, C. Liu and S. Luo, *Electrochem. Commun.*, 2011, **13**, 133–137.

58 C. Schatz, C. Pichot, T. Delair, C. Viton and A. Domard, *Langmuir*, 2003, **23**, 9896–9903.

59 F. Zouaoui, S. Bourouina-Bacha, M. Bourouina, N. Jaffrezic-Renault, N. Zine and A. Errachid, TrAC, *TrAC, Trends Anal. Chem.*, 2020, 115982.

60 P. Hashemi, N. Karimian, H. Khoshsafar, F. Arduini, M. Mesri, A. Afkhami and H. Bagheri, *Mater. Sci. Eng., C*, 2019, **102**, 764–772.

61 M. Goumri, C. Poilâne, P. Ruterana, B. B. Doudou, J. Wéry, A. Bakour and M. Baitoul, *Chin. J. Phys.*, 2017, **2**, 412–422.

62 D. Sangamithirai, V. Narayanan, B. Muthuraaman and A. Stephen, *Mater. Sci. Eng., C*, 2015, **55**, 579–591.

63 S. K. Sahoo and A. Mallik, *NANO*, 2015, **02**, 1550019.

64 T. F. Emiru and D. W. Ayele, *Egypt. J. Basic Appl. Sci.*, 2017, **1**, 74–79.

65 M. Rostami, M. Rahimi-Nasrabadi, M. R. Ganjali, F. Ahmadi, A. F. Shojaei and M. Delavar Rafiee, *J. Mater. Sci.*, 2017, **12**, 7008–7016.

66 M. Ciszewski, A. Mianowski, P. Szatkowski, G. Nawrat and J. Adamek, *Ionics*, 2015, **21**, 557–563.

67 E. Laviron, *J. Electroanal. Chem. Interfacial Electrochem.*, 1979, **1**, 19–28.

68 A. Gopalakrishnan, N. Vishnu and S. Badhulika, *J. Electroanal. Chem.*, 2019, **834**, 187–195.

69 Y. Zhao, X. Zheng, Q. Wang, T. Zhe, Y. Bai, T. Bu and L. Wang, *Food Chem.*, 2020, **333**, 127495.

70 P. Wei, Z. Zhu, R. Song, Z. Li and C. Chen, *Electrochim. Acta*, 2019, **317**, 93–101.

71 L. Wang, H. Zhu, H. Hou, Z. Zhang, X. Xiao and Y. Song, *J. Solid State Electrochem.*, 2012, **4**, 1693–1700.

72 D. Han, T. Han, C. Shan, A. Ivaska and L. Niu, *Electroanalysis*, 2010, **22**, 2001–2008.

73 L. Wang, Y. Zheng, X. Lu, Z. Li, L. Sun and Y. Song, *Sens. Actuators, B*, 2014, **195**, 1–7.

74 X. Wang, M. Wu, W. Tang, Y. Zhu, L. Wang, Q. Wang and Y. Fang, *J. Electroanal. Chem.*, 2013, **695**, 10–16.